The effect of blockage on power production for laterally aligned wind turbines

A R Meyer Forsting[1], N Troldborg[1]

[1] DTU Wind Energy, Department of Wind Energy, Technical University of Denmark, Risø Campus, DK-4000 Roskilde, Denmark

E-mail: `alrf@dtu.dk`

Abstract. This paper studies the change in the individual power coefficients for a laterally aligned row of wind turbines over a single, free turbine in the context of varying inflow directions via numerical simulations. All turbines were rotating in-line with the main flow direction. The problem definition is similar to that of many wind turbine testing sites and wind farms. Hence any changes in the individual turbine power production could have implications regarding power curve validation procedures.These changes are relatively small and therefore the size of the computational domain was identified to be detrimental in avoiding any domain-inflicted blockage. Increasing the misalignment of the main flow direction with the row of turbines led to significant variations in the power production across turbines. At the largest inflow angle of 45° it varied from -1.1 % to 2 %. As a whole, the power production increased by about 0.5 %, almost independent of the inflow direction.

1. Introduction

The lateral spacing between wind turbines is an important parameter in wind farm development, as it limits the number of wind turbines for a given site. Recent technological advances in the wind turbine industry have left many prime wind farm sites underperforming to their power production potential, due to their older, sub-MW turbines. Many wind parks have to undergo extensive modernisation programs in the years to come. These include upgrading to taller towers and larger rotors. In most cases, however the tower positions are fixed under the initial planning permits. As a consequence the lateral distance between blade tips is further reduced. Moving rotors ever more closely together means that the individual blockage effects, that are caused by the pressure jump across turbines, start to interact. Therefore the velocity field upstream is not only altered locally for a single turbine but, also on the global, wind farm scale. One would hence expect significant patterns to emerge in the individual power coefficients. Performance analyses of wind farms, though mainly focusing on wake effects, reveal significant variations along the first row of wind turbines, even if their causation has not so far been identified [1].

Whereas the effect might be negligible over an entire wind farm they can be significant in turbine power curve verification. Wind turbine testing sites normally align several turbines so that they lie on an axis perpendicular to the prevailing wind direction. Representative of this are the DTU sites Høvsøre and Østerild in Denmark. The widely used IEC standard for power curve validation does not include any specifications regarding lateral spacing, instead focusing on the avoidance of wake interaction from neighbouring objects and other turbines. Depending on the layout of the testing site valid wind sectors might include wind directions of up to 45° to the

alignment axis. The underlying assumption is of course that the neighbouring wind turbines are not influencing each other significantly, even at large inflow angles. Evaluating and quantifying the power production under the effect of interacting blockages, thus may proof important for future testing procedures and standards, as these assumptions are tested. In particular the influence on short-range remote sensing technology could be significant as it relies heavily on quantifying the local velocity field upstream.

Blockage has attracted most attention in marine research, as it has been shown experimentally [2] and numerically [3, 4] that it significantly increases the power output of tidal wave turbines. This conclusion is not transferable to wind turbines, which operate in a free domain unrestricted by water depth. In wind energy the focus has been largely on longitudinal spacing and wind farm staggering, as these parameters significantly influence wake interaction. Its impact on overall wind farm power production and turbine lifetime explain the proliferation of papers published on this subject. Previous attempts to quantify upstream blockage in a wind engineering context heavily relied on low Reynolds number experiments and a limited number of flow conditions. This includes work of Medici *et al.*, who used hot-wire anemometry and particle image velocimetry on a single turbine and concluded that blockage was noticeable more than three turbine diameters (D) upstream [5]. McTavish *et al.* studied the effect with similar limitations for three turbines by attempting to reach power maximization through an optimal spatial arrangement [6]. A power increase of 8 % was observed for a lateral spacing of 1.5D during experiments, which was validated by vortex particle simulations.

None of the current literature quantifies the blockage effect to the extent that any conclusions could be drawn for wind turbine testing. All existing experiments' flows were operating at small Reynolds numbers and the flow orientation was at all times perpendicular to the line of turbines. Furthermore the impact of tunnel blockage on results was hastily rejected and not properly assessed. The approach of this paper is more systematic. It employs computational fluid dynamics (CFD) to evaluate any kind of blockage and more specifically its possible effects on power curve measurements, where special attention is given to uncertainty reduction.

1.1. Problem definition

To allow for the conclusions of this paper to be relevant for turbine testing procedures, the arrangement adopted is loosely related to the DTU Høvsøre testing site. As shown in figure 1.1 five turbines are aligned on an axis with a 3D lateral spacing. Taking current measuring procedures as a reference, the angle between the line of wind turbines and the main wind direction (θ) was varied from $0°$ to $45°$ in $15°$ steps and the wind speed set to 8 ms^{-1}. Note that θ will sometimes be referred to as 'yaw' in the following passages. The inflow was set to be uniform and the solution assumed to be time invariant.
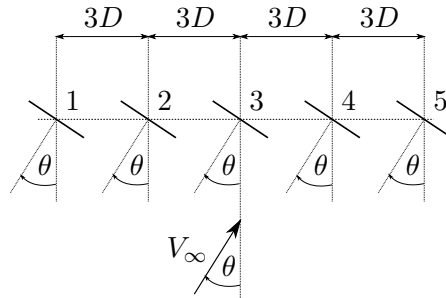

Figure 1. Schematic of the wind turbines' arrangement and reaction to changing inflow directions.

2. Computational method

2.1. Flow solver

The finite volume code EllipSys3D solves the incompressible Reynolds Averaged Navier-Stokes (RANS) equations over a discretised block-structured domain [7–9]. The SIMPLE algorithm [10] solves the pressure-linked terms of the Navier-Stokes equations, while the QUICK scheme [11] is applied to the convective terms. To allow the implementation of discrete body forces without jeopardising the coupling between velocity and pressure a modified Rhie-Chow algorithm has been implemented [12]. Further the Menter $k-\omega$ shear-stress transport modelled the turbulence [13].

2.2. Turbine model

Allowing the computations to be easily reproducible and representative of wind turbines currently employed, the well known NREL 5-MW [14] turbine with a diameter of 126 m was used. At the set wind speed of 8 ms^{-1}, the rotor performs 9.21 rotations per minute (RPM).

In the computational domain the rotor is represented by permeable body forces, which are derived from local velocity and 2-D airfoil data. In this particular simulation the actuator shape model [15] distributed these forces inside the domain by calculating the intersection between the rotor and flow grid.
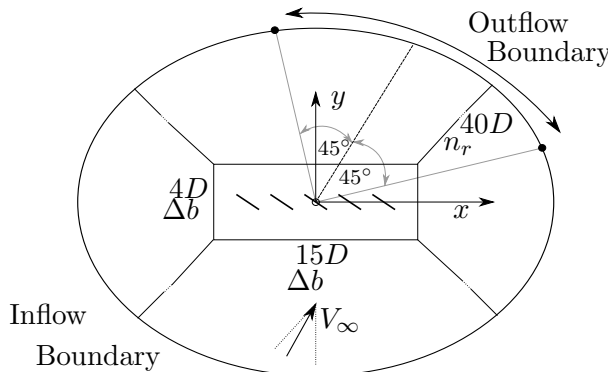
2.3. Numerical domain

Figure 2. Top view of the numerical domain. All dimensions are scaled by the turbine diameter D. Note that the boundaries are a function of the inflow angle.
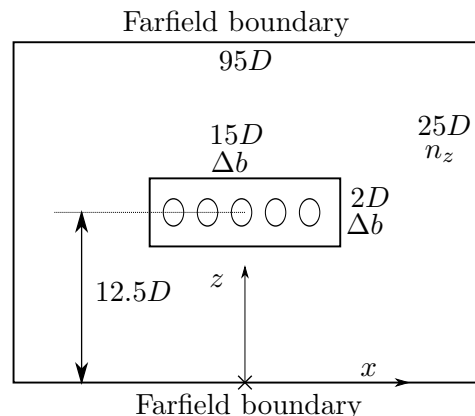

Figure 3. Frontal view of the numerical domain.

2.3.1. Layout The numerical domain was discretised by a structured O-type meshing methodology, containing a centrally located equispaced box mesh. The latter encompassed the row of turbines. Farfield boundary conditions were applied to both, top and bottom of the domain. The inflow and outflow boundaries were applied dynamically to the sides of the O-mesh by the preprocessor, depending on the inflow angle. More specifically the outflow sector is $\pm$ 45° centred around the inflow direction. A schematic layout of the domain and its coordinate system is shown in figures 2 and 3. All dimensions were scaled by D. The spacing inside the central box was fully defined by the inner grid spacing Δb, that resulted from the number of grid points specified per diameter (n_{rot}). From there the mesh grew hyperbolically outwards in the radial and z directions, where the dimension of the first cell connecting to the inner box mesh

was equal to Δb. The number of grid spaces along the radial and z directions were defined by n_r and n_z respectively.

2.3.2. Grid resolution and domain size To allow the conclusions drawn from this paper to be generally applicable, the grid resolution had to be sufficiently fine and the domain large enough to ensure the simulation results to be independent of these two factors.

Preliminary investigations showed that a relatively large domain was needed with respect to other types of investigations, to avoid 'tunnel' blockage influencing the results. 'Tunnel' blockage refers to constriction of the cross-sectional area through an object, leading to flow acceleration, which will hence influence the C_P of each turbine. In fact the equivalent 'tunnel' blockage, if defined as the rotor swept area over the cross-sectional area of the numerical domain, was 0.165 %, much lower than was seen as acceptable in previous investigations [6]. To further reduce the uncertainty deriving from the domain size, an outflow correction can be implemented at the domain boundaries to remove some of the excess mass flow. Koning [16] worked with potential flow assumptions to show that an analytical solution can be obtained to estimate this outflow. Here the actuator disc is represented by a doublet pressure source, which determines the flowfield everywhere. The final outflow velocity induced by a single turbine in the local disc coordinate system, denoted by $\bullet'$, is given as:

$$u_i' = \frac{1}{2}aV_\infty \frac{R^2 x_i'}{\left(\sum_{i=1}^{3} x_i'^2\right)^{3/2}} \text{ with } x_i' = \{x'y'z'\} \text{ and } u_i' = \{u'v'w'\} \tag{1}$$

,where a is the axial induction factor and R the disc radius. The former is estimated by momentum theory ($C_T = 4a(1-a)$) [17], where the thrust coefficient (C_T) is taken from a non-corrected simulation. Note that applying this correction is to a certain extent equivalent to increasing the domain size. No correction is needed for unrestricted domain methods.

The following paragraph addresses the second important factor regarding the discritisation of the domain and its influence on the results. As previously mentioned the changes in the C_P to be investigated were assumed to be relatively small, thus already at the first grid iteration, the resolution was aimed to be high. For wake investigations setting the number of points per diameter (n_{rot}) to 8, results in an acceptably low error [18]. Here it was initially set to 32, instead. In table 1 a summary of all grid parameters is presented. A higher grid level derived from halving the inner box spacing Δb.

Table 1. Mesh parameters.

Mesh	n_{rot} $[D^{-1}]$	Δb $[D]$	n_r	n_z	Cells $_{\times 10^6}$
coarse	32	0.0313	32	128	2.05
fine	64	0.0156	64	256	8.21

Since the intention of this paper is to investigate the variation of C_P along a row of turbines, its sensitivity to changes in the domain size and grid level was analysed to evaluate the uncertainty in the simulations. The minimum and maximum yaw (θ) settings were chosen as evaluation points, as these were expected to yield the most extreme simulation solutions, making grid and domain errors more noticeable.
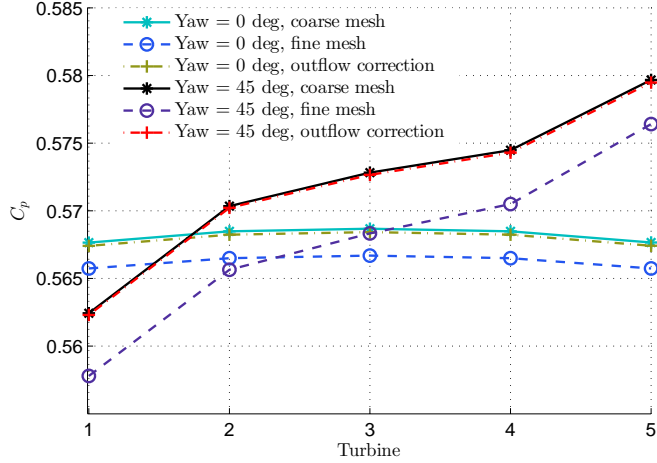
Figure 4. Evolution of C_P along a row of turbines for a coarse, fine and coarse mesh with outflow correction.

In figure 4 the evolution of C_P with turbine number is presented for the fine, coarse and coarse mesh with the outflow correction at the two extreme yaw positions. All curves agree in terms of their overall trend, though there is a visible offset between the solutions of the coarse and fine meshes. A numerical summary of the grid and domain errors is presented in table 2. The errors are calculated by taking the non-corrected coarse mesh solution as base and then calculating the resulting percentage difference in C_P at each turbine. As the aim of this study is to access relative changes in C_P across the row of turbines any absolute offsets are acceptable as long as they stay constant across the row. This implies that its standard deviation ($\sigma(\Delta C_P)$) has to be small. Between the fine and coarse meshes the largest error in predicting the overall trend was 0.1 %. This is acceptable for proving a significant change in C_P and therefore the coarse mesh was sufficiently resolved. The outflow correction had an even smaller impact, thus showing that the domain was acceptably large.

Table 2. Grid and domain errors calculated with the coarse mesh solution for C_P as base.

	θ [°]	$\langle \Delta C_P \rangle$ [%]	$\sigma(\Delta C_P)$ [%]
Grid	0	0.344	0.00636
	45	0.738	0.11200
Outflow	0	0.0433	0.000928
	45	0.0272	0.005070

2.4. Turbine orientation and location correction
The power coefficient for each turbine is not independent of its grid location. Therefore single turbine calculations are needed at each turbine location. Furthermore yawing the turbines inside the numerical domain (see figure 2) changes the way the body forces from the actuator disc are implemented inside the flow domain, thus making single turbine calculations at each yaw setting necessary. The resulting C_P values are then used to normalise the simulations:

$$\Delta C_P|_{i,j} = \frac{C_P|_{i,j} - C_{P_{single}}|_{i,j}}{C_{P_{single}}|_{i,j}} \times 100$$

$$\text{,with } i = \{1, \dots, 5\}, j = \{0, 15, \dots, 45\}$$

(2)

3. Results

3.1. Power evolution

Figure 5 shows the variation in the global power coefficient across the row of turbines for the four inflow settings. These results are summarised in figure 6 in terms of their respective mean, minimum and maximum at each inflow angle. For a yaw of 0° the result's overall trend agrees well with those of McTavish [6]. McTavish also found an increased mean power production and a rise towards the centre of the row. A direct comparison is not possible as his lateral spacing was only 1.5D, half of what is used in this simulation. Yawing the inflow changes the behaviour markedly. Whereas the middle turbine (3) shows an increase in the power production close to the mean value, the upstream turbines (1-2) are losing their gain in power in line with an increase in yaw. For the first turbine losses are observed from a yaw of 15° onwards. The losses upstream are counteracted by almost equally sized increases on the downstream side (4-5). The existing balance between the losses upstream and gains downstream is underlined by the mean of all turbines being practically independent of yaw (see figure 6).
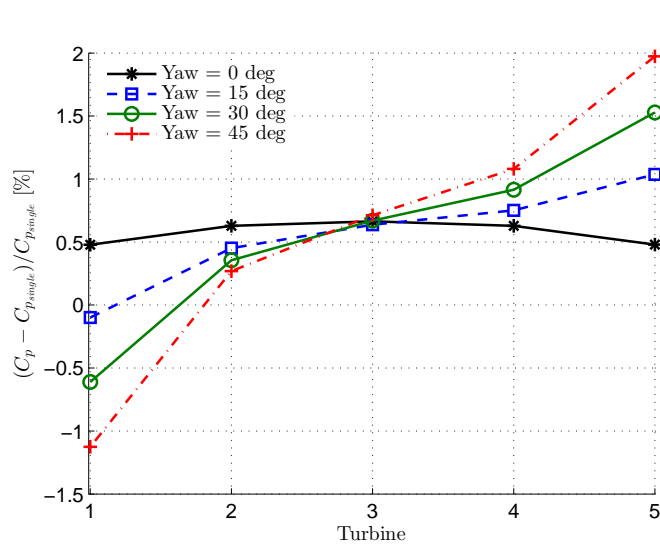

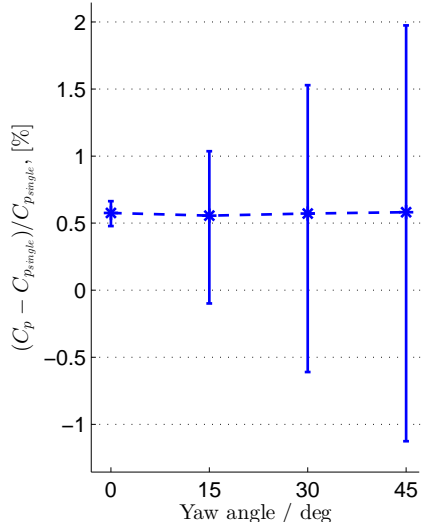**Figure 5.** Percentage change in the power coefficient for different yaw angles.

Figure 6. Summary of mean, minimum and maximum values of the results in figure 5 as a function of yaw angle.

3.2. The flowfield

The changes in the power coefficient along a row of turbines presented in the previous section can be directly linked to the emerging flow phenomena.

The main factors that are interacting and causing these flow alterations are the blockage, both on a local and global scale, and the acceleration of the flow between wind turbines and neighbouring wakes. The overall flow alterations are best explained via the extreme example of

$\theta = 45°$. Contours of the free-stream normalised axial velocity component (v_a) for this case are shown in figure 7. All wind turbines taken together act as one large flow obstruction and thus cause the emergence of a 'global' blockage effect or, equivalently, induction zone. Its presence is clearly visible in figure 7, where the flow is decelerating over the entire length of the wind farm. Notably at a yaw of 45° this deceleration is visibly reduced along the row of turbines.
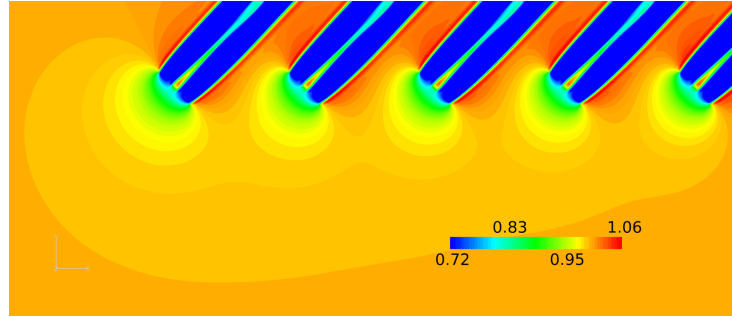

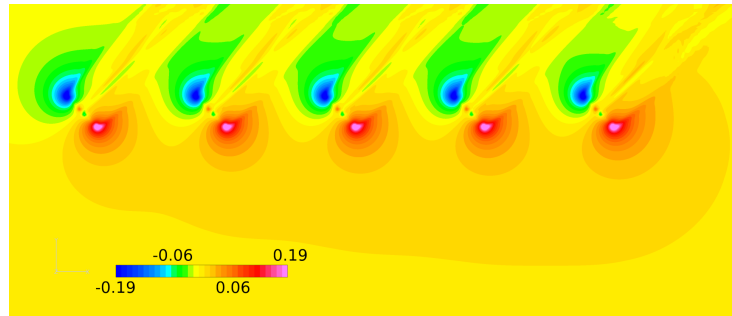**Figure 7.** Normalised axial velocity contours (v_a) at a yaw angle (θ) of 45°.

Figure 8. Normalised cross flow velocity contours (u) at a yaw angle (θ) of 45°.

This can be partly attributed to the local blockage from each turbine. As the flow approaches the turbine furthest upstream (1) the local induction reduces the mass flow forcing some of the flow to be diverted around it and thus towards turbine 2. There some of the flow is channelled through the space between the neighbouring wake and the turbine, hence causing the flow to accelerate, reducing the size of the local induction zone of turbine 2. This is also reflected by the axial velocity v_a distributions along the disc for turbines 3 and 5 shown in figure 9. This flow diversion continues all along the row of turbines leading to a continues build up of mass flow, as not all the excess flow escapes in-between turbines and wakes. This build up is a clear feature in the cross flow velocity contours in figure 8. It is this effect that leads to a decrease in the global induction zone along the row of turbines, as the flow accelerates. Note that the axial forcing from the turbines, defined by the thrust coefficient C_T, is actually increasing towards turbine 5. This shows that it is indeed the acceleration causing the decrease in the global induction zone. The process described in the paragraph above is aggravated by an increase in θ, as the distance between the turbines and neighbouring wakes decreases. This reduces the mass flow in-between turbines and wakes, causing an increase in the cross flow. Linked to this decrease in distance is a stronger induction felt by turbine 1 (see figure 9). The increased induction at turbine 1 and the subsequent increase in v_a along the row can be better understood by conceiving the row of turbines as a partially permeable flat plate.
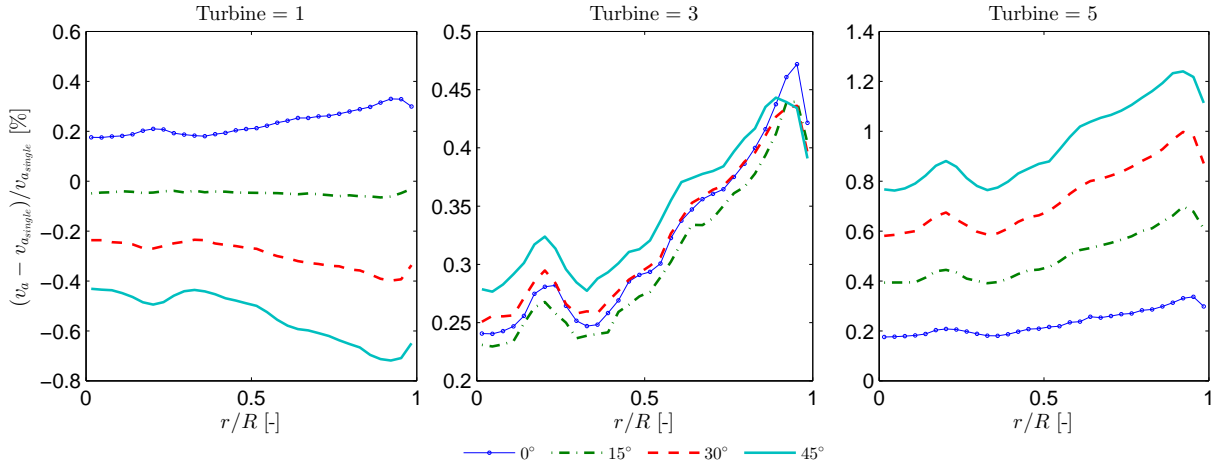
Figure 9. Azimuthally averaged axial velocity v_a distributions at the rotor disc at each yaw configuration.

4. Conclusion

The blockage effect and its impact on power production were assessed for a scenario similar to that of a wind turbines testing site using CFD. Extensive attention was paid to uncertainty reduction by assessing the influence of the numerical methodology on the results. Detrimental to a reliable investigation of this rather small effect, was selecting a sufficiently large domain. As an outcome the blockage ratio was significantly lower than deemed usually acceptable at 0.165 %. It is generally recommended to use similar ratios for domain restricted methods or alternatively applying corrections.

The blockage effect for laterally aligned wind turbines significantly alters the upstream flow, leading to marked changes in individual power coefficients. An inflow orthogonal to the row of turbines only had limited impact, causing a mean increase in the power coefficient across all turbines of 0.57 %. The different turbines' C_P values encompassed a range of 0.18 %. Yawing the inflow in respect to the line of alignment did not greatly affect the mean, in contrast to this the range of C_P extended in line with turbine rotation up to 3.1 % at 45°.

This was attributed to local and global blockage effects. Global blockage increased with turbine rotation, making the row of turbines adopt flow characteristics similar to those of a flat plate, diverting increasing amounts of mass flow down the row of turbines. Furthermore a stronger induction zone appeared at the upstream turbine causing a decrease in power, whereas downstream reacceleration lead to increases, peaking at the last turbine (2.0 % at 45°).

For wind turbine testing sites the accuracy with which a power performance evaluation can be carried out is of utmost importance. Even relatively small changes in the individual power coefficients, registered in this study, might prove significant. Nevertheless to make specific recommendations for real world applications, a more realistic flow, including an atmospheric boundary layer should be implemented and the actual measurement procedure be included.

References

[1] Mitraszewski K, Hansen K, Nygaard N and Rethoré P E Wall effects in offshore wind farms *Torque 2012*

[2] Bahaj A, Molland A, Chaplin J and Batten W 2007 *Renewable Energy*

[3] Turnock S R, Phillips A B, Bank J and Nicholls-Lee R 2011 *Ocean Engineering*

[4] Nishino T, Richard and Wilden H 2012 *J. Fluid Mech.*

[5] Medici D, Ivanell S, Dahlberg J A and Alfredsson P 2011 *Wind Energy*

[6] McTavish S, Rodrigue S, Feszty D and Nitzsche F 2014 *Wind Energy* DOI: 10.1002/we.1806

[7] Sørensen N 1995 *General purpose flow solver applied to flow over hills* Ph.D. thesis RisøNational Laboratory

[8] Michelsen J 1994 Basis3d - a platform for development of multiblock pde solvers Tech. rep. Dept. of Fluid Mechanics, Technical University of Denmark, DTU

[9] Michelsen J 1994 Block structured multigrid solution of 2d and 3d elliptic pdes Tech. rep. Dept. of Fluid Mechanics, Technical University of Denmark, DTU

[10] Patanker S and Spalding D 1972 *International Journal of Heat and Mass Transfer*

[11] Leonard B 1979 *Computer Methods in Applied Mechanics and Engineering*

[12] Rethoré P E and Sørensen N 2012 *Wind Energy*

[13] Menter F R 1993 *AIAA Journal*

[14] Jonkerman J, Butterfield S, Musial W and Scott G 2009 Definition of a 5-mw reference wind turbine for offshore system development Tech. rep. NREL

[15] Rethoré P E, van der Laan P, Troldborg N, Zahle F and Sørensen N 2014 *Wind Energy*

[16] 1976 *Aerodynamic Theory: A General Review of Progress* (Peter Smith) chap Devision M: Influence of the propeller on other parts of the airplane structure

[17] 2008 *Aerodynamics of Wind Turbines 2nd Ed.* (Earthscan)

[18] van der Laan P, Sørensen N N, Rethoré P E, Mann J, Kelly M C, Troldborg N, Schepers J G and Machefaux E 2014 *Wind Energy*